JOURNAL OF PROPULSION AND POWER
Vol. 26, No. 1, January–February 2010

Technical Notes

One- and Three-Dimensional Wall Heat Flux Calculations in a O_2/H_2 System

Aravind Vaidyanathan*
Iowa State University, Ames, Iowa 50011
and
Jonas Gustavsson† and Corin Segal‡
University of Florida, Gainesville, Florida 32611

DOI: 10.2514/1.44640

I. Introduction

OVER the past several decades, considerable effort has been dedicated to model combustion in rocket chambers to understand and predict the conjugate heat transfer to the chamber walls [1]. Validation of computational fluid dynamics (CFD) design tools requires, in turn, reliable experimental data assessment. This involves the need to acquire a comprehensive set of data in the same facility, including wall heat fluxes along with inflow measurements over a broad range of pressures [2].

The experimental data for CFD validation acquired to date were obtained from a range of facilities of different sizes, various internal geometry or fuel composition, and injection configurations [3–9]; therefore, wall heat fluxes were considerably different among these studies. The strength, the life cycle, and the cooling system effectiveness are highly dependent on heat transfer into and out of the system [10], and the number of studies addressing the heat transfer into the chamber walls are still inadequate.

In a previous study, which was the first of its kind, Marshall et al. [11] obtained the heat flux measurements using Gordon heat flux gauges from coaxial temperature measurements that were placed along the chamber wall. The heat fluxes were, then, calculated by solving the transient axisymmetric heat flux equation. Conley et al. [12] calculated the heat fluxes from the temperature measurements at several longitudinal locations. In these studies, the heat fluxes were calculated by solving the steady-state one-dimensional (1-D) heat conduction equation and adding a correction term to compensate the heat absorption by the chamber walls. The very nature of heat transfer in the combustion chamber is, in fact, three-dimensional (3-D). Thus, calculation of heat fluxes based on a 1-D assumption may lead to errors. Vaidyanathan et al. [13] calculated wall heat fluxes by numerically solving the two-dimensional (2-D) unsteady heat conduction equation. Although more accurate when compared with 1-D assumption, the 2-D heat conduction assumption still does not take into account the longitudinal heat transfer.

Received 30 March 2009; revision received 15 June 2009; accepted for publication 9 July 2009.

*Post Doctoral Research Associate, Department of Mechanical Engineering. Member AIAA.
†Post Doctoral Research Associate, Department of Mechanical and Aerospace Engineering. Member AIAA.
‡Associate Professor, Department of Mechanical and Aerospace Engineering; cor@ufl.edu. Associate Fellow AIAA.

The current study is aimed at calculating the heat fluxes in the combustion chamber by numerically solving the 3-D heat conduction equation to assess the validity of 1-D unsteady heat conduction assumption in wall heat flux calculation. Hence, the data presented next include wall heat fluxes calculated from 3-D heat transfer assumption for a GO_2/GH_2 single-element shear coaxial injector at 37 bar.

II. Experimental Details

A high-pressure combustion experimental facility with a single shear GO_2/GH_2 injector was used here. The facility described in detail in [5,6] can operate at pressures up to 60 bar. The chamber configuration and injector details are also detailed in [5,6]. The oxidizer is injected into the chamber through the center tube, whereas the fuel is injected through the annular region surrounding it. The pressure in the current study was selected to be 37 bar. The oxidant-to-fuel (O/F) mass ratio was 3.79, and the velocity ratio was 0.4. This resulted in a hydrogen exit velocity of 103.5 m/s for a mass flow of 0.58 g/s. The experiments lasted for 8 s following ignition.

For heat transfer measurements, thermocouples are embedded in the side chamber walls with two thermocouples at each longitudinal location. Exposed-tip thermocouples with a response time of 15 ms were used here. The depth location of the thermocouples at any chamber cross section is shown in Fig. 1. For each thermocouple pair, the temperatures are measured at 3.2 and 9.5 mm from the inner chamber walls, respectively. The temperature at a location 3.2 mm from the inner wall is denoted as T_{inner}, and the temperature measured at 9.5 mm is denoted as T_{middle}.

The longitudinal locations of the heat flux thermocouples, identified as HF1 to HF8, along the chamber wall length are given in Table 1, with the injector face taken as the reference.

III. Heat Flux Calculation and Results

The wall heat fluxes were determined from the temperature measured in the chamber wall, first by solving the steady-state 1-D heat conduction equation and adding a correction term to compensate the heat absorption by the chamber as shown in

$$q_A = \frac{k}{\Delta x}(T_{i,2} - T_{o,2}) + \frac{\rho C \Delta x}{2}\left(\frac{T_{o,2} - T_{o,1}}{\Delta t}\right) \tag{1}$$

where q_A is the heat flux, Δx is the distance between the thermocouple pairs, the subscript i is assigned for the thermocouple close to the inner chamber wall, the subscript o represents the one farthest from the inner chamber wall, and 1 and 2 represent the initial and final times, respectively. Here, as in the previous studies [11,12], the heat fluxes were calculated by assuming the effect of the longitudinal heat conduction as negligible. As the very nature of the heat transfer in the

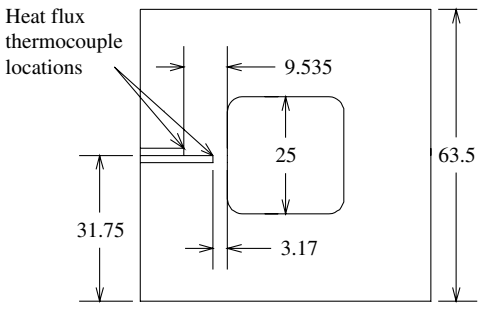

Fig. 1 Depth location of heat flux thermocouples (dimensions in mm).

Table 1 Location of heat flux thermocouples along the chamber wall

Heat flux thermocouple	Distance from injector face, mm
HF1	27.6
HF2	37.7
HF3	47
HF4	58
HF5	70
HF6	89.1
HF7	102.2
HF8	112.4

combustion chamber is 3-D in the current study, the heat flux was calculated second by numerically solving the unsteady 3-D heat conduction equation and compared with the heat flux calculation based on a 1-D assumption.

A 3-D model of the central portion of the chamber from 37 to 102 mm from the injector face was chosen as the computational domain. The central portion of the chamber was selected, because the temperature measured outside of this domain indicated that the longitudinal temperature gradient can be assumed negligible. The outer wall was assumed to be insulated, such that the heat released during the experiment was assumed to be entirely accumulated in the chamber wall. The validity of the insulated wall assumption was checked by imposing forced convection at the outer walls, assuming the outer wall temperature to be at 100°C and the ambient air temperature to be set at 27°C. Forced convection was calculated by assuming an air velocity of 10 m/s. These conditions are considerably more dissipative than experienced during the experiments. The heat transfer for the case of a laminar forced convection past a flat plate with the prescribed values was, then, calculated and was found to amount to 0.1% of the heat flux values in the chamber walls due to combustion; therefore, all the heat released during the transient process was assumed to accumulate in the walls.

The computational temperatures and their slopes, which evolved over the period of 8 s, were matched with the actual temperatures, and their slopes were obtained from the experimental run at the thermocouple locations. The imposed heat flux at the inner chamber walls was changed for different sets of computation, so that the temperatures T_{inner} and T_{middle} obtained from the computations matched the experimental results within 5 to 6°C. The discretized 3-D heat conduction equation used here was [14]:

$$\frac{k}{(\delta x)^2}(T_{i+1,j,l,t} - 2T_{i,j,l,t} + T_{i-1,j,l,t}) + \frac{k}{(\delta y)^2}(T_{i,j+1,l,t} - 2T_{i,j,l,t} + T_{i,j-1,l,t}) + \frac{k}{(\delta z)^2}(T_{i,j,l+1,t} - 2T_{i,j,l,t} + T_{i,j,l-1,t}) = \frac{\rho C}{\delta \tau}(T_{i,j,l,t+\delta\tau} - T_{i,j,l,t}) \tag{2}$$

Here, the density ρ and the heat capacity C for copper (110) are 8700 kg/m^3 and 385 J/(kg K), respectively. The grid independent computational domain consisted of a $141 \times 141 \times 141$ grid, and the time step was 0.0001 s. The initial condition consisted of the inner and middle temperatures: T_{inner} and T_{middle} set at an ambient temperature of 27°C. A variation of ±2°C in the initial temperature condition resulted in a maximum uncertainty of less than 1% in imposed heat flux values and hence is considered negligible.

The axial temperatures recorded at the end of 8 s for both the inner and middle locations along the chamber wall are plotted in Fig. 2, and the longitudinal gradient in the upstream of 37 mm and downstream of 102 mm locations are assumed negligible, thereby selecting the 37 to 102 mm domain for analysis.

For every time step, the temperature surface boundary condition at 37 and 102 mm was obtained by solving the 2-D heat conduction

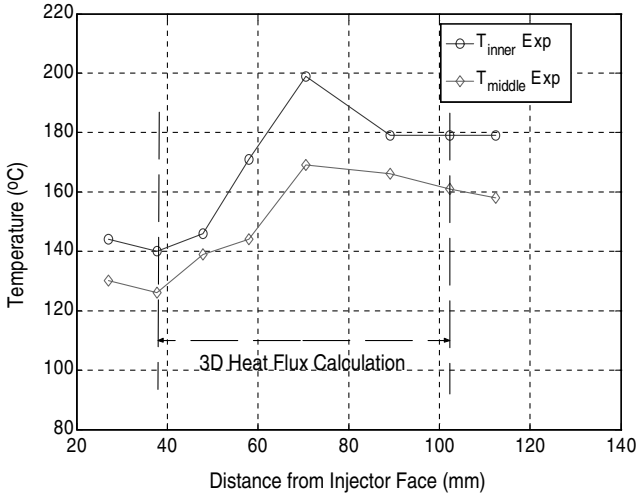

Fig. 2 Chamber wall temperatures at inner and middle locations along the chamber wall at the end of the 8 s.

equation and assuming longitudinal conduction upstream of 37 mm and downstream of 102 mm to be negligible as aforementioned. The assumption of longitudinal heat conduction upstream of 37 mm and downstream of 102 mm as negligible was chosen as a first step toward calculating and comparing the heat fluxes from 1-D and 3-D heat transfer assumptions. However, in future studies aimed at refining the data, the possibility of substituting the negligible longitudinal heat conduction at 37 and 102 mm surface boundary conditions with a constant or variable longitudinal heat conduction could be explored. The discretized 2-D heat conduction equation used here was [14]:

$$\frac{k}{(\delta x)^2}(T_{i+1,j,t} - 2T_{i,j,t} + T_{i-1,j,t}) + \frac{k}{(\delta y)^2}(T_{i,j+1,t} - 2T_{i,j,t} + T_{i,j-1,t}) = \frac{\rho C}{\delta \tau}(T_{i,j,t+\delta\tau} - T_{i,j,t}) \tag{3}$$

The evolution of heat flux with time was assumed to be an exponential function with time $[1 - \exp(t)]$ to match the experimental temperatures as well as the slopes of the temperature rise. The judicious selection of an exponential function for heat flux evolution was based on the observation from the chamber pressure rise with time. The chamber pressure rise indicated that, in the beginning of the test, the inlet propellant mass flow rates are higher than the exit mass flow rates of product gases, resulting in accumulation of mass in the chamber. As the test progressed in time, the inlet and exit mass flow rates gradually equalized, and the chamber attained a steady state. Thus, the heat flux to be imposed at the inner chamber walls should also follow a similar trend, and hence an exponential evolution in time was assumed. The heat flux was subjected to iteration until the experimental and computational temperatures matched within 5–6°C.

The grid independence was evaluated by varying the grid size of the computational domain from $51 \times 51 \times 51$ to $101 \times 101 \times 101$ and $141 \times 141 \times 141$. The increase in the imposed heat flux values as the 3-D grid size was increased from 51 to 101 was 4.3%, and for the 3-D grid size increased from 101 to 141, the increase was 2.8%. This indicated that the computations are nearly grid independent at a grid size of 141.

The heat fluxes thus determined in the axial direction are shown in Fig. 3 along with the heat flux calculated from the linear and unsteady term assumption in Eq. (1). The heat flux values and the time constant in the heat flux evolution [i.e., $\tau_c = 1 - \exp(-\alpha t)$] were varied, such that all the experimental and computational temperatures could still be matched within 5–6°C. The analysis was done toward the end of the 8 s sequence, when the experimental conditions reached steady state.

The heat fluxes thus determined from the 3-D computational analysis had a maximum variation of less than 2% when the

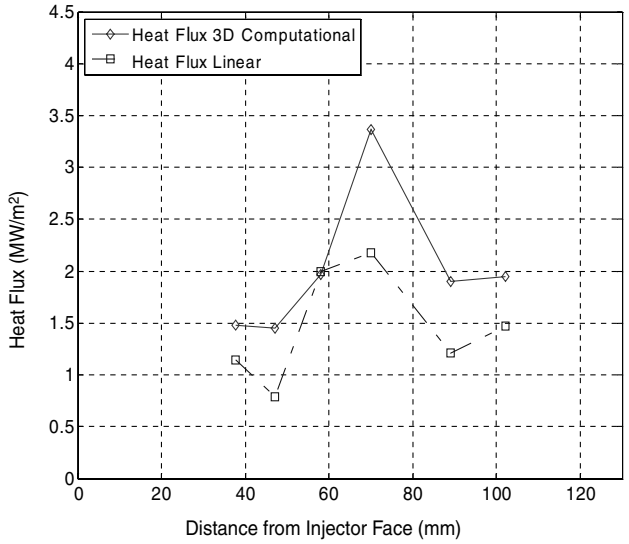

Fig. 3 Chamber wall heat fluxes calculated based on 3-D computations and the linear and unsteady assumption at 37 bar.

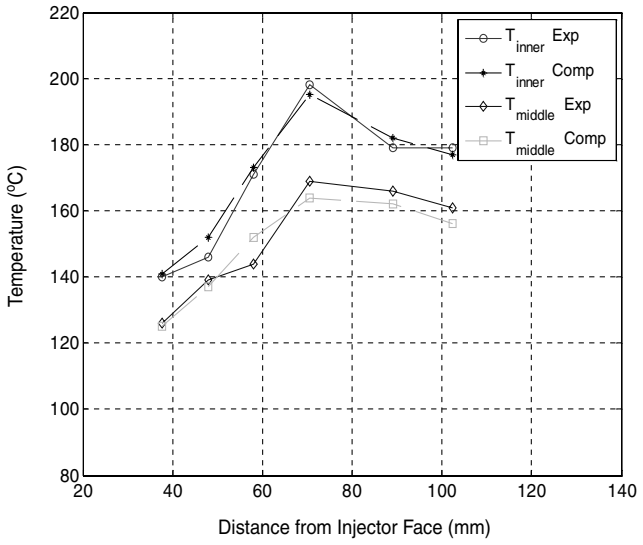

Fig. 4 Computational and experimental temperatures for 37 bar at the end of 8 s.

experimental and computational temperatures were matched within 5–6°C. It can be seen from Fig. 3 that both calculations based on 3-D computations and linear assumption showed the same qualitative trend, but the heat fluxes determined from the latter was relatively lower. The peak value of heat flux determined from the 1-D heat flux calculations is 35% lower than the corresponding peak value from the 3-D heat flux calculation. This shows that the effect of the longitudinal heat conduction cannot be neglected, and its contribution must be included in the heat flux measurements and flow calculations.

The heat flux has a peak value at 70 mm, indicating the location of shear layer reattachment. The matching of experimental and computational temperatures at the end of 8 s for 37 bar are also shown in Fig. 4. The difference of 5–6°C as convergence criteria was adopted as a first step in determining the validity of the 1-D heat conduction assumption, which was not attempted in any of the work aimed at providing heat fluxes for validating computational models in rocket injector studies. The variation in the computational parameters and the difference of 5–6°C for temperature matching are areas that can be investigated in future studies.

IV. Conclusions

This study generated a comprehensive database of wall heat fluxes for GH_2/GO_2 combustion at an O/F mass flow ratio of 3.77 and chamber pressures of 37 bar. The comparison between heat fluxes calculated from linear and 3-D analysis showed that the peak value predicted by the latter is 35% higher than the former. The assumption of linear heat conduction in combustion chamber walls may lead to errors in heat flux calculations; hence, the 3-D assumption is recommended for future studies.

Acknowledgments

This work has been performed with support from the NASA Constellation University Institute Project. We thank Claudia Meyer, the program manager. The authors would like to acknowledge the continuous support offered by K. Tucker (NASA Marshall) and J. Hulka (Jacobs Sverdrup).

References

[1] Zurbach, S. (ed.), Rocket Combustion Modeling, 3rd International Symposium, Centre National D'Etudes Spatiales, Paris, March 2006.

[2] Tucker, K., West, J., Williams, R., Lin, J., Rocker, M., Canabal, F., Robles, B., and Garcia, R., "Using CFD as a Rocket Injector Design Tool: Recent Progress at Marshall Space Flight Center," NASA NTRS 20050217148, Jan. 2005.

[3] Allen, M. G., and Miller, M. F., "Optically-Accessible Gas Turbine Combustor for High Pressure Diagnostics Validation," AIAA Paper 97-0116, Jan. 1997.

[4] Kojima, J., and Nguyen, Q.-V., "Development of a High-Pressure Gaseous Burner for Calibrating Optical Diagnostic Techniques," NASA TM-2003-212738, 2003.

[5] Carter, C. D., King, G. B., and Laurendeau, N. M., "A Combustion Facility for High-Pressure Flame Studies by Spectroscopic Methods," *Review of Scientific Instruments*, Vol. 60, No. 8, 1989, pp. 2606–2609. doi:10.1063/1.1140679

[6] Locke, R. J., Hicks, Y. R., Anderson, R. C., and Ockunzzi, K. A., "OH Imaging in a Lean Burning High-Pressure Combustor," *AIAA Journal*, Vol. 34, No. 3, 1996, pp. 622–624. doi:10.2514/3.13113

[7] Foust, M. J., Deshpande, M., Pal, S., Ni, T., Merkle, C. L., and Santoro, R. J., "Experimental and Analytical Characterization of a Shear Coaxial Combusting GO_2/GH_2 Flowfield," AIAA Paper 96-0646, Jan 1996.

[8] Santoro, R. J., "Applications of Laser-Based Diagnostics to High Pressure Rocket and Gas Turbine Combustor Studies," AIAA Paper 1998-2698, June 1998.

[9] Singla, G., Scouflaire, P., Rolon, C., and Candel, S., "Planar Laser-Induced Fluorescence of OH in High Pressure Cryogenic LO_x/GH_2 Jet Flames," *Combustion and Flame*, Vol. 144, Nos. 1–2, 2006, pp. 151–169. doi:10.1016/j.combustflame.2005.06.015

[10] Tramecourt, N., Masquelet, M., and Menon, S., "Large-Eddy Simulation of Unsteady Wall Heat Transfer in a High Pressure Combustion Chamber," AIAA Paper 2005-4124, July 2005.

[11] Marshall, W. M., Pal, S., Woodward, R. D., and Santoro, R. J., "Benchmark Wall Heat Flux Data for a GO_2/GH_2 Single Element Combustor," AIAA Paper 2005-3572, July 2005.

[12] Conley, A., Vaidyanathan, A., and Segal, C., "Heat Fluxes Measurements in a GO_2/GH_2 Single-Element, Shear Injector," *Journal of Spacecraft and Rockets*, Vol. 44, No. 3, 2007, pp. 633–639. doi:10.2514/1.26678

[13] Vaidyanathan, A., Gustavsson, J., and Segal, C., "Heat Fluxes/OH-PLIF Measurements in a GO_2/GH_2 Single-Element Shear Injector," AIAA Paper 2007-5591, July 2007.

[14] Chapman, A. J., *Fundamentals of Heat Transfer*, Macmillan, New York, 1987.

D. Talley
Associate Editor